

Manganese-based metal-organic frameworks-oxidized multi-walled carbon nanotube composites for determination of Pb²⁺ and Cd²⁺

Sisi Chen^a, Runmin Huang^a, Kuan Luo^a, Jingang Yu^{a,b}, Xinyu Jiang^{a,b,*}

^aSchool of Chemistry and Chemical Engineering, Central South University, Changsha 410083, China, emails: jiangxinyu@csu.edu.cn (X. Jiang), 1102763799@qq.com (S. Chen), 89010456@qq.com (R. Huang), 1752359201@qq.com (K. Luo), yujg@csu.edu.cn (J. Yu)

^bKey Laboratory of Hunan Province for Water Environment and Agriculture Product Safety, Changsha 410083, China

Received 4 January 2019; Accepted 15 May 2019

ABSTRACT

An oxidized multi-walled carbon nanotubes-metal organic framework composite (OM-MOF) was prepared by solvothermal synthesis methods and characterized by Fourier infrared spectroscopy, X-ray diffraction (XRD), scanning electron microscopy and thermogravimetric analysis. The prepared material was subsequently applied in simultaneous electrochemical detection of Pb²⁺ and Cd²⁺. Electrochemical impedance spectroscopy and cyclic voltammetry were performed for electrochemical characterization. Some experimental conditions such as material concentration, buffer solution types, buffer pH, deposition potential and deposition time have been explored. Under optimum conditions, electrochemical detection and application were carried out, where good linear (0.05–5 μM) and sensitivity (4.96 μA/μM for Pb²⁺ and 3.07 μA/μM for Cd²⁺), were obtained. Meanwhile, the detection limit for Pb²⁺ and Cd²⁺ was 13 and 38 nM, respectively.

Keywords: Oxidized multi-walled carbon nanotubes; Metal organic framework; Lead ions; Cadmium ions; Electrochemical detection

1. Introduction

Because of the biological toxicity and hard degradation, heavy metals are identified as one of the most representative water pollutants [1]. In some cases, the heavy metals generate a variety of pernicious forms through physical or chemical process, which are hard to control and bring great potential pitfalls to environment and organisms. Lead and cadmium ions are two typical heavy metals that can bring disease when beyond a certain amount. The major sources of lead pollution come from coal, metallurgical and other industries, while cadmium pollution mainly comes from the chemical industry, smelting industry and waste incineration [2,3]. Many life examples show that the heavy metals do bring great detriment to human life, so monitoring of heavy metal ions is a hot topic that is worth being studied.

Nowadays, many methods are applied to detect heavy metal ions, such as inductively coupled plasma mass spectrometry, surface enhanced Raman spectroscopy [4], atomic absorption spectrometry, and electrochemical method. In recent years, electrochemical method has attached great attention owing to its low cost, simple operation and fast response [5], which has been used for the determination of biological small molecule, organic dye, antibiotic, heavy metal ions and so on. To detect heavy metal ions, anodic stripping voltammetry has been applied, which can detect several metal ions simultaneously and hold high sensitivity [6,7]. However, owing to the small specific area, limited active sites and low adsorption capacity of bare electrode, many modified materials such as carbon nanotubes (CNTs), graphene nanosheets (GNS), and activated carbon have been used in electrochemical detection. Meanwhile, some novel

* Corresponding author.

materials such as metal organic framework (MOF), metal oxide, and metal sulfide have been used for electrocatalytic oxidation or reduction. In addition, many new materials with high surface area, good adsorption capacity and excellent conductivity have also been produced for electrode modification [8–12].

MOF is a kind of inorganic material with large specific surface area, rich holes and controllable morphology, which present excellent performances on catalysis, adsorption, separation, etc. Recently, many MOF materials have been used in electrode modification. For example, Gou et al. [13] has synthesized an amino-functionalized Ni (II)-based MOF applying in Pb^{2+} detection, where good linear range of 0.5–6 μM and significant detection limit of $5.08 \times 10^{-7} \text{ M}$ has been obtained. Wang et al. [14] have prepared $\text{UiO-66-NH}_2@ \text{PANI}$ for Cd^{2+} monitor. In their work, wide detection range of 0.5–600 mg L^{-1} and laigh detection limit about 0.3 mg L^{-1} have been achieved, which indicates that MOF materials has wide application prospects in electrochemical detection. However, poor conductivity is a drawback for MOF materials, which greatly impede its development. To ameliorate this deficiency, some carbon materials including CNTs, GNS, and fullerenes were usually used.

CNTs, a class of one-dimensional carbon material, including single-walled carbon nanotubes (SWCNTs) and multi-walled carbon nanotubes (MWCNTs), are usually used as electrode materials because of their large specific surface area, excellent electrical conductivity and chemical stability [15,16]. For example, the $\text{MWCNTs}@ \text{Cu}_3(\text{BTC})_2$ has been synthesized and applied for lead monitor with detection range from 1.0×10^{-9} to $5.0 \times 10^{-8} \text{ M}$ and excellent detection limit of $7.9 \times 10^{-10} \text{ M}$ [17]; Moreover, comparing with SWCNTs, MWCNTs own many unique merits: low cost, high stability, considerable defects (accelerates electron transfer and enhances electrochemical response) and good grooming ability. Functional MWCNTs are more widely used than unembellished CNTs. For instance, carbon-based electrodes, coated by Ag or Au nanoparticles decorated MWCNTs, were synthesized by Guzsány et al. [18], which were applied for amperometric determination of H_2O_2 ; A polydopamine-multiwalled carbon nanotube material was prepared by Shahbakhsh et al. [19], which were used for determination of biocompounds within biological fluids environment; Ahmad et al. [20] synthesized a zinc-layered hydroxide-L-phenylalanate-modified MWCNT as a paste electrode material for electrochemical detection of paracetamol. In their work, low limit of $8.3 \times 10^{-8} \text{ M}$ was achieved. Among all functional MWCNTs, oxidized MWCNTs (OM) is a class of simple, dispersible high performance materials.

Oxidized MWCNTs (OM), possessing rich functional groups (carboxyl and epoxy) and good electrical conductivity, were usually used as electrode material because of their excellent complexation with heavy metals. In this work, oxidized MWCNTs-MOF composite (OM-MOF) was prepared. Meanwhile, pure OM and MOF were synthesized as a comparison. The composite (OM-MOF) owned the advantages of both OM and MOF. Differential pulse anodic stripping voltammetry recorded from -1 to -0.3 V was applied for simultaneous electrochemical analysis of

lead and cadmium ions. All works in this experiment were conducted at room temperature.

2. Experimental

2.1. Reagents

Potassium permanganate (KMnO_4 , $\geq 99.5\%$) was provided by Tianjin Kermel Chemical Reagent Co. Ltd., Tianjin, China. MWCNTs (main range of diameter: 20–40 nm, length $> 5 \mu\text{m}$, purity $> 97\%$) were purchased from Shenzhen Nanotech Port Co. Ltd., Shenzhen, China. Zinc nitrate hexhydrate ($\text{Zn}(\text{NO}_3)_2 \cdot 6\text{H}_2\text{O}$, $\geq 99\%$), anhydrous manganese chloride (MnCl_2 , $> 99\%$), anhydrous sodium sulfite (Na_2SO_3 , $\geq 97\%$), concentrated nitric acid (HNO_3) and terephthalic acid ($> 99\%$) were produced by Shanghai Chemical Reagent Co. Ltd., Shanghai, China. Sodium acetate (CH_3COONa , $> 99\%$) and acetic acid (CH_3COOH , $w \geq 99.5\%$), used as supporting electrolytes, were obtained from Sinopharm Chemical Reagent Co. Ltd., Shanghai, China. N,N-Dimethylformamide (DMF, $> 99.5\%$) was acquired from Chengdu Organic Chemistry Co. Ltd., Chengdu, China. Water used in this work was ultrapure, produced by a Milli-Q water purification system (Millipore, Milford, MA). All the reagents used were of analytical grade and were not purified further before use.

2.2. Synthesis of OM-MOF and MOF

The Ox-MWCNTs were prepared according to a previous method [16,21] with some modification. 0.3 g of KMnO_4 and 20 mL of HNO_3 were mixed first, and then 200 mg MWCNTs were added into the above mixture. After that, the mixture was heated to 100°C and lasted for 6.5 h. As the mixture cool to room temperature, slight overdose of Na_2SO_3 was dropped into it until no bubbles appeared. Then, the Ox-MWCNTs were purified by vacuum filtration and washed until the pH was close to 7, and vacuum drying followed.

20 mL of DMF was employed to dissolve 2 mg of Ox-MWCNTs, kept ultrasound for 5 min, and then 0.126 g of MnCl_2 and 0.148 g of $\text{Zn}(\text{NO}_3)_2 \cdot 6\text{H}_2\text{O}$ were put into the above solution. The mixture solution was subjected to ultrasound for another 5 min. Meanwhile, the ligand solution was obtained by dissolving 0.357 g of terephthalic acid (TPA) in 10 mL of DMF, which was then slowly dropped into metal ion solution with continuous stirring. The final solution was stirred overnight and poured into a 45 mL Teflon liner for 24 h at 120°C . The precipitate was washed by water, and dried overnight at 60°C . The MOF was synthesized by the same process with no Ox-MWCNTs added.

2.3. Modification of working electrode

First, 2 mg of prepared OM-MOF and 1 mL of water were blended to form a uniform solution (ultrasound 10 min). Second, the bare glassy carbon electrodes were burnished (by means of 0.05 μm alumina slurry) and washed by ultrapure water. Third, electrodes were ultrasonic cleaned for about 2 min under ultrapure water. After that the cleaned glassy carbon electrodes were modified by dropping 8 μL prepared material solution on their mirror-like face and dried at ambient temperature. The OM/GCE and MOF/GCE were framed

through the alike process. Some apparatus used in this work were displayed in supporting material.

2.4. Apparatus

Some instruments and measurements were used to characterize materials. Voltammetric measurements were carried out on a CHI660E Electrochemical Workstation (Chenhua Instrument Co. Ltd., Shanghai, China) with a three-electrode system, where modified electrode acted as working electrode, Ag/AgCl electrode was the reference electrode while counter electrode was a platinum wire. The Fourier transform infrared (FT-IR) was performed on a Nicolet 6700 FT-IR spectroscopy. To explore the surface morphologies of modified materials, field emission scanning electron microscopy (FE-SEM, MIRA3 TESCAN) was used. Thermogravimetric analysis (TGA) was performed from 0°C to 800°C on an SDT Q600 V8.0 Build 95 thermal analyzer with a heating rate 10°C min⁻¹ under N₂ atmosphere. XRD patterns were obtained by Rigaku D/max 2550. Cyclic voltammetry (CV) measurements were recorded from -0.2 to 1.0 V while differential pulse voltammetry (DPV) measurements were recorded from -1 to -0.3 V with a pulse amplitude of 50 mV and a pulse width of 60 ms. The electrochemical impedance measurements were carried out in a solution of 1.0 mM K₃[Fe(CN)₆]/K₄[Fe(CN)₆] containing 0.1 M KCl with the frequency range from 1 to 10⁶ Hz.

3. Results and discussion

3.1. Characterization of materials

The XRD diagram of MOF and OM-MOF are shown in Fig. 1. Many intensity and sharp peaks could be observed easily from the figure, which indicated that the MOF had excellent crystal structure. Some characteristic peaks were marked such as 2θ = 9.63°, 14.30°, 18.32°, and 19.33°, which corresponded to the (200), (110), (101), and (111) planes, respectively. Meanwhile, the standard XRD pattern (CCDD number 771995) was used to match these peaks. The result

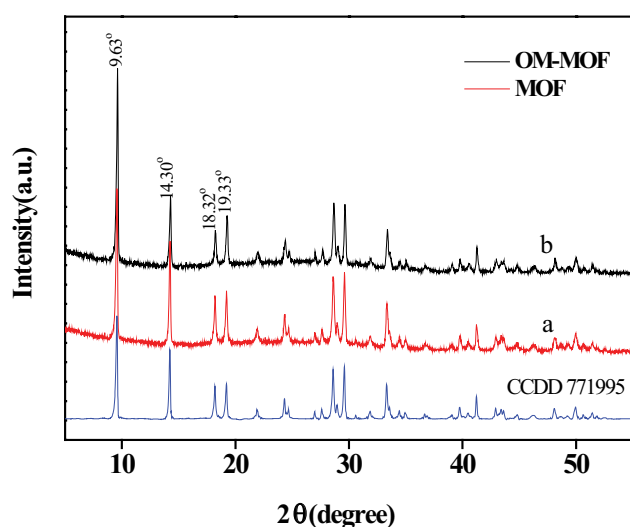


Fig. 1. XRD patterns of (a) MOF and (b) OM-MOF.

displayed that all the diffraction peaks presented above could be found from the standard XRD pattern, which manifested that the presence of Ox-MWCNTs did not affect the crystallinity of the material.

The FT-IR curves of MOF, OM-MOF and OM are shown in Fig. 2. For curve of OM-MOF, many absorption peaks could be observed. At 1,632.44 and 1,383.61 cm⁻¹ were appeared two obvious absorption peaks which were respectively corresponding to asymmetric and symmetric stretching for COO⁻. At 3,388.50 cm⁻¹ was a wide and deep absorption peak, which matched with the telescopic vibration of -OH. Moreover, the vibration of benzene ring was embodied in the absorption bands at 1,508.09 cm⁻¹; 1,543.74 and 817.18 cm⁻¹. Assuredly, the absorption peaks that relative to the vibration of O-Mn-O were arisen at 543.32, 507.46, and 426.20 cm⁻¹. Additionally, compared with MOF (curve a), all characteristic absorption peaks could be observed on OM-MOF (curve b) but a little shift appeared from 1,546.65 and 1,386.59 to 1,543.74 and 1,383.66 cm⁻¹ indicating π-π interaction and hydrogen bonding between OM and MOF. Certainly, the absorption intensity of OM-MOF was stronger than OM but weaker than MOF.

The SEM images of OM-MOF and MOF in high magnification and low magnification are shown in Fig. 3. Under low magnification, the material looked like a little disorganized (picture C, D) but in good shape. The MOF (picture A, C) was a long strip laminated stack with slightly distinct geometric shape. From picture B, it was obviously observed that OM dispersed in the MOF material. The morphology of OM-MOF was inconsistent with the literature report [21], which might attribute to the presence of zinc ions during the synthesis. But the EDX draw (Fig. 4) shows that there were no zinc ions been found in the final OM-MOF material (although two metal ions: Zn²⁺ and Mn²⁺ were added simultaneously), which might result from weaker binding ability between zinc ions and phthalic acid (especially when the amount of organic ligand was insufficient). In spite of no zinc ions were appeared in modified material, there was a hypothesis that the adding of zinc ions could affect the

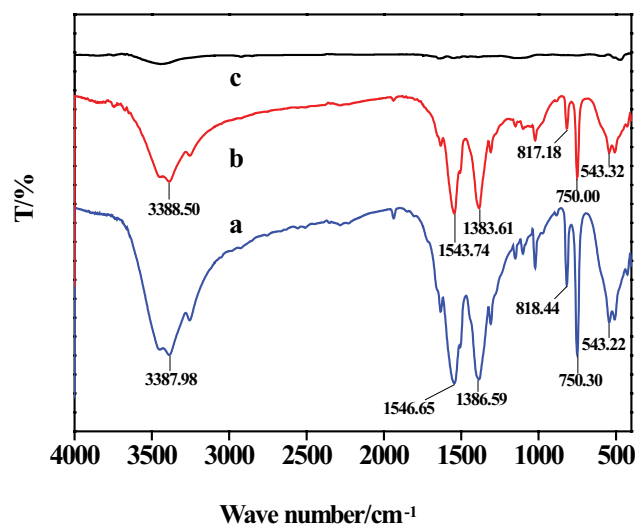


Fig. 2. FT-IR spectra of (curve a) MOF, (curve b) OM-MOF, and (curve c) OM.

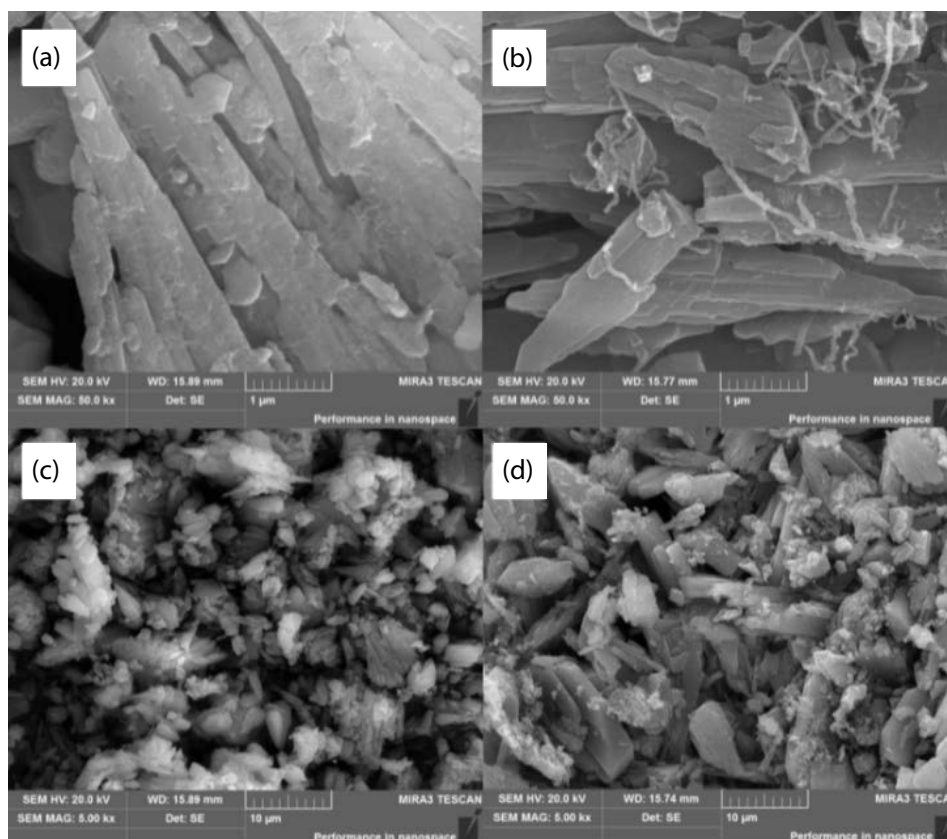


Fig. 3. SEM images of (a, c) MOF and (b, d) OM-MOF in (a, b) high magnification and (c, d) low magnification

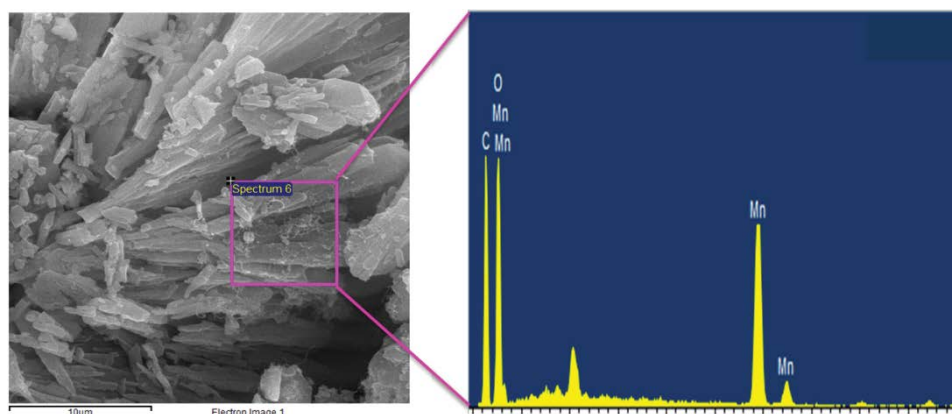


Fig. 4. EDX diagram of OM-MOF.

morphology and electrochemical performance of OM-MOF. To confirm this hypothesis, the pure OM-MOF (No zinc ions were added during the synthesis) was synthesized and the current signal was tested (Fig. 5). The lower response and uglier curve of pure OM-MOF indicated that zinc ions played an important role in the formation of OM-MOF.

The thermogravimetric curves of OM and OM-MOF are shown in Fig. 6. There just appeared 11.01% loss for OM when the temperature increased to 800°C but 67.41% loss for OM-MOF. The curve for OM was relatively flat from 0°C to 800°C but the curve for OM-MOF had two sharp

drops. The first weight loss (~12.18%) could be observed when the temperature increased from 121.5°C to 165.7°C, which was corresponding to the release of DMF molecules that existing in the channels or coordinating with the metal center; the second weight change (~39.52%) appeared when the temperature arrived 456.9°C, which was ascribed to the decomposition of organic framework. Finally, when the temperature came to 571.0°C, the material was large-scale thermal destroyed. The dates present above indicated that the modified material owns meglio stability and could be used in room temperature.

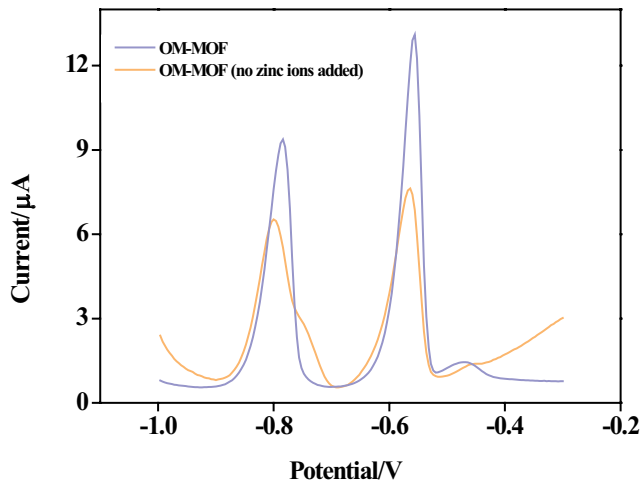


Fig. 5. Current signal of pure OM-MOF and OM-MOF (deposition time: 300 s; deposition potential: -1.2 V; signal recorded: -1 to -0.3 V; ions concentration: $3 \mu\text{M}$; Supporting electrolyte: 0.1 M NaAc-HAc).

3.2. Electrochemical behavior of modified GCE

For the sake of exploring the electrochemical behavior of different modified electrodes, cyclic voltammetry (CV), electrochemical impedance spectroscopy (EIS) and differential pulse anodic stripping voltammetry (DPASV) were applied. The CV and EIS were conducted on Bare/GCE, OM/GCE, MOF/GCE and OM-MOF/GCE under 1.0 mM $[\text{Fe}(\text{CN})_6]^{3-/4-}$ (1:1) solution containing 0.1 M KCl (Fig. 7a). It was obvious that MOF/GCE and OM-MOF/GCE produced greater redox current than bare/GCE and OM/GCE, suggesting that the modified materials had good electrical conductivity. But when it came to peak spacing, MOF/GCE had largest peak-to-peak separation, the poor electron transfer rate of MOF material may account for this phenomenon. For OM-MOF/GCE, it had smaller peak separation than MOF/GCE, showing that the addition of Ox-MWCNTs could

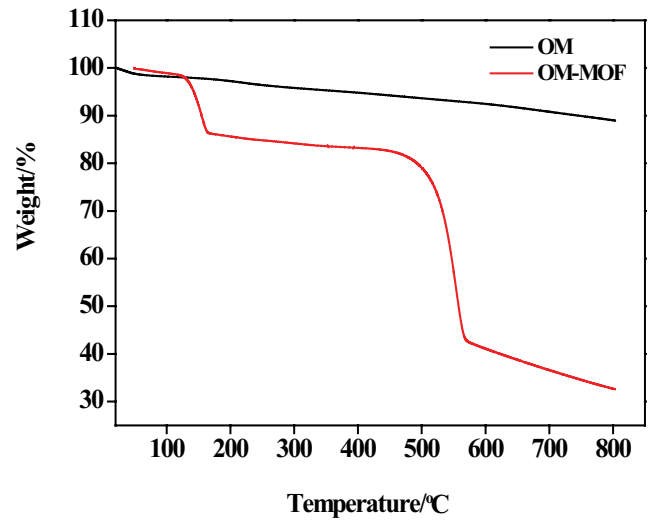


Fig. 6. Thermogravimetric curves of OM and OM-MOF.

largely improve its electron transfer rate. The EIS curve of Bare/GCE, OM/GCE, MOF/GCE and OM-MOF/GCE are shown in Fig. 7b. The OM/GCE showed the minimum resistance about 96.14Ω . The resistance of bare/GCE, MOF/GCE, and OM-MOF/GCE were very similar, about 120.1Ω , 123.3Ω and 109.2Ω , respectively, which were corresponding to CV curves. The DPV curves for different electrodes are shown in Fig. 8. The MOF/GCE showed poor electrochemical response to Pb^{2+} and Cd^{2+} mainly because of the poor electron transfer rate. Obviously, the current response of OM/GCE was poorer than that of OM-MOF/GCE and showed a better performance to Cd^{2+} , which was attributed to the stronger complexation between COO^- and Cd^{2+} . Compared with the bare GCE, the OM-MOF/GCE exhibited better electrochemical response, almost 5 times to Pb^{2+} and 7 times to Cd^{2+} , and the peaks of OM-MOF/GCE were more beautiful than those of OM/GCE. Thus, the OM-MOF was chosen as electrode modified material.

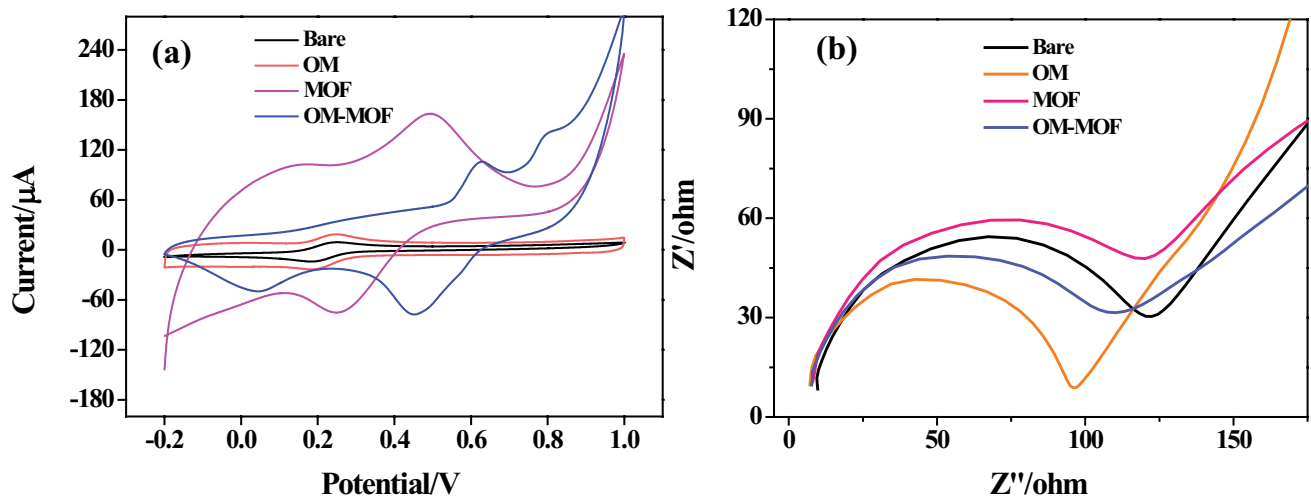


Fig. 7. (a) Cyclic voltammetry (CV) curves of bare/GCE, OM/GCE, MOF/GCE and OM-MOF/GCE and (b) EIS curves of bare/GCE, OM/GCE, MOF/GCE, and OM-MOF/GCE.

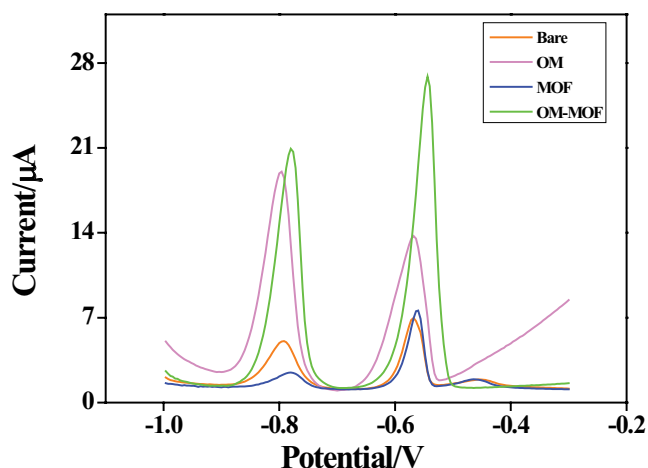


Fig. 8. Differential pulse voltammograms of 5 μM Pb^{2+} and Cd^{2+} at different modified electrodes in 0.1 M sodium acetate buffer (pH = 4.0).

3.3. Optimizing operation conditions

In order to exhibit the best response, some experimental conditions were optimized, including material concentration, buffer solution types, buffer pH, deposition potential and deposition time. The material concentration was a pretty important factor to improve peak response (Fig. 9a). The peak response increased with the increasing of material concentration (from 1 to 2 mg mL^{-1}), which might attributed to the enrichment of binding sites. However, once the material concentration above 2 mg mL^{-1} , the current response began to decrease, suggesting that the coating was too thick to promote the electron transformation.

The type of buffer solution is another decisive factor for electrochemical response. Four common buffer solutions were explored in this work (Fig. 9b). NaAc-HAc (ABS) showed the biggest peak strength, which meant that ABS had fastest electron transfer rate and the most suitable ion stabilization for Pb^{2+} and Cd^{2+} . The pH of buffer solution could not be ignored in electrochemical determination because the process of protonation and deprotonation for modified material and hydrolysis of metal ions in alkaline environment were tightly related with pH value. In this experiment the pH value changed from 3 to 7. From Fig. 9c, the current response for Pb^{2+} aggrandized with the increasing of pH value from 3 to 5 but decreased dramatically when $\text{pH} > 5$. While, the current intensity for Cd^{2+} been highest when $\text{pH} = 4$ but decreased sharply when $\text{pH} = 5$, which might be mainly influenced by the existence of Pb^{2+} , because of the competition between Pb^{2+} and Cd^{2+} . For this reason, $\text{pH} = 4$ was chosen for this work.

Deposition potential and deposition time are two conditions that need to be investigated. Generally speaking, the longer the deposition time lasts, the greater the current intensity presents. But for deposition potential, different metal ions have different optimal deposition potential. In this experiment, the deposition time was changed from 60 to 360 s and the deposition potential was explored from -0.8 to -1.3 V. As exhibited in Fig. 9d, the highest response appeared at -1.2 V for both Pb^{2+} and Cd^{2+} and a lower

response at a more negative or corrected potential. Fig. 9e is the deposition time-current diagram. For Pb^{2+} , with the increasing of deposition time, the peak current increased, which was corresponding to the general experience. But when it came to Cd^{2+} , something different appeared. As the accumulation time exceeds 300 s, the current value began to decrease. This phenomenon was also caused by the competition between Pb^{2+} and Cd^{2+} . The sites on the electrode surface were limited, as the deposition time increased; the electrode surface became saturated gradually. Due to the difference potential, lead ions were more likely to deposit on the electrode surface, so the response of cadmium ions in 360 s was lower than 300 s. Considering all these factors, the best experiment conditions were chosen: material concentration: 2 mg mL^{-1} ; supporting electrolyte: NaAc-HAc; optimal pH: 4.0; deposition time: 300 s; deposition potential: -1.2 V. All tests in this experiment were performed under optimal conditions.

3.4. Differential pulse voltammetry determination of Pb^{2+} and Cd^{2+}

Under optimal conditions, the relationship between metal ions concentration and current response was investigated on OM-MOF/GCE. To investigate the mutual influence between Pb^{2+} and Cd^{2+} , the selective detection was conducted by keeping one ion concentration constant and increasing another ion concentration. As presented in Fig. 10a, the voltammetric response of Cd^{2+} enlarged with the rising Cd^{2+} amount (from 0.05 μM to 3 μM) in the existence of 0.3 μM Pb^{2+} and the linear equation of Cd^{2+} was $I (\mu\text{A}) = 1.487 C (\mu\text{M}) - 0.1027$ ($R^2 = 0.991$). Little oxidation current changed for 0.3 μM Pb^{2+} with the increase of Cd^{2+} . Similarly, the DPV stripping signal of Pb^{2+} , in the presence of 0.5 μM Cd^{2+} , increased with the increase of Pb^{2+} amount (from 0.05 to 5 μM) and the calibration curve of Pb^{2+} was shown in Fig. 10b. It was clear that little response changed for Cd^{2+} with the increase of Pb^{2+} amount. The acquired linear equation of Pb^{2+} was $I (\mu\text{A}) = 1.738 C (\mu\text{M}) + 0.6144$ with the correlation coefficient (R^2) of 0.999. The results suggested that there was little mutual interference between the two ions. Following, the simultaneous detection of Pb^{2+} and Cd^{2+} was conducted by synchronously increasing ion concentration of Pb^{2+} and Cd^{2+} . As shown in Fig. 10c and d, the linear equation was $I (\mu\text{A}) = 4.960 C (\mu\text{M}) - 0.06476$ and $I (\mu\text{A}) = 3.103 C (\mu\text{M}) - 0.1209$ for Pb^{2+} and Cd^{2+} , respectively. The detection limit ($S/N = 3$) for Pb^{2+} and Cd^{2+} was 13 and 38 nM and the sensitivity for Pb^{2+} and Cd^{2+} was 4.96 and 3.07 $\mu\text{A}/\mu\text{M}$, respectively, which reached the safety values for drinking water prescribed by WHO ($\text{Pb}^{2+} \leq 48\text{nM}$, $\text{Cd}^{2+} \leq 38\text{nM}$). In addition, compared with some previous reports (shown in Table 1), wide linear response (from 0.05 to 5 μM) and low detection limit (13 nM for Pb^{2+} and 38 nM for Cd^{2+}) were obtained in this work. Meanwhile, the electrode material we used was relatively simple, inexpensive, stable and environmental friendly.

3.5. Interference and stability study

To investigate the anti-interference ability of the modified electrode, different kinds of possible interfering cations and anions were affiliated to supporting electrolyte containing

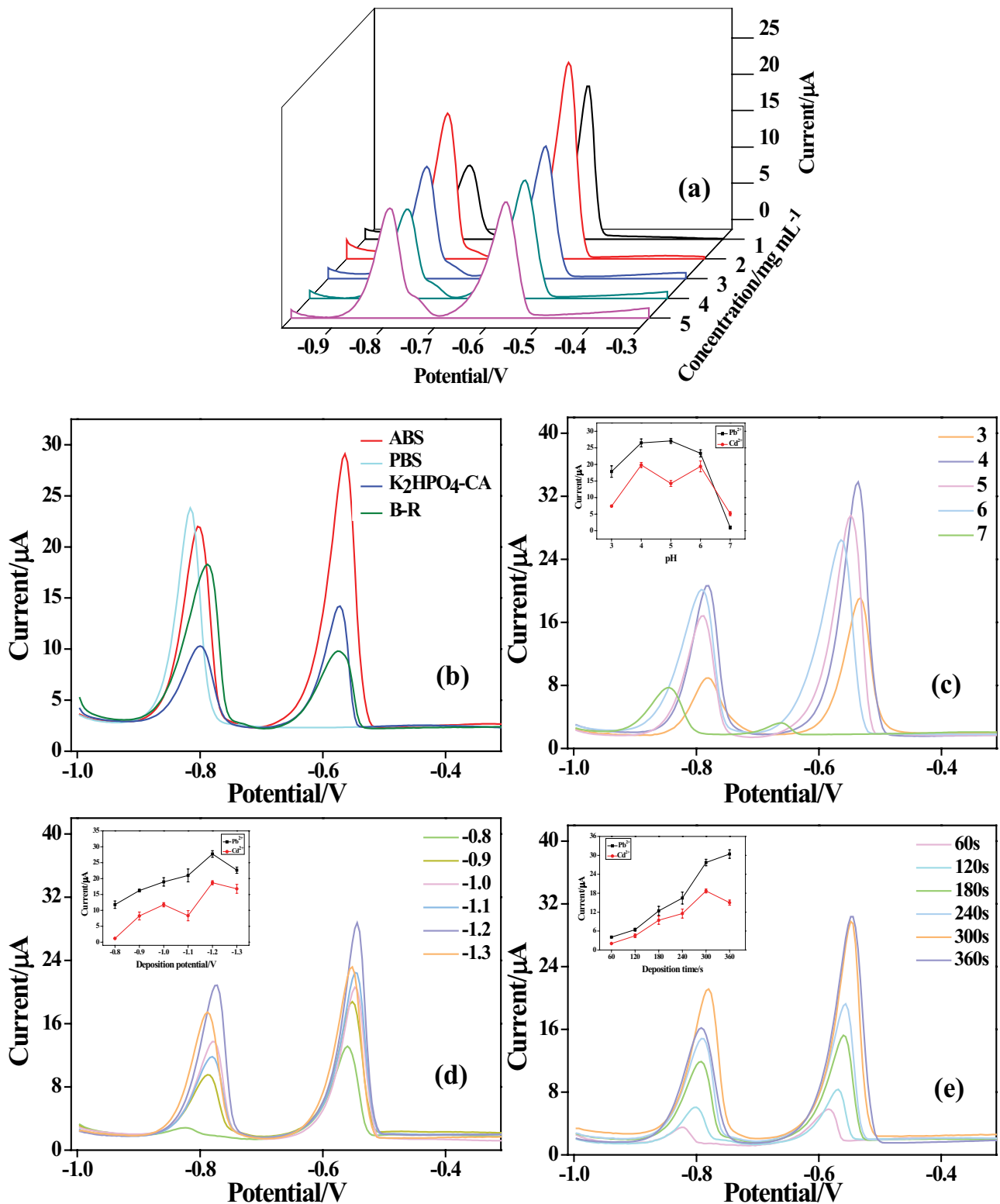


Fig. 9. (a) Different electrode responses for different material concentrations (the dropping amount for each electrode was 8 μL.), (b) current responses for different supporting electrolytes (NaAc–HAc, Na₂HPO₄–NaH₂PO₄, K₂HPO₄–CA, Britton–Robinson buffer), (c) current responses of Pb²⁺ and Cd²⁺ in different pH. Inset: the calibration curve of Cd²⁺ and Pb²⁺ in different pH, (d) DPASV responses of Pb²⁺ and Cd²⁺ in different deposition potential. Inset: the calibration curve of Cd²⁺ and Pb²⁺ in different deposition potential, and (e) DPASV responses of Pb²⁺ and Cd²⁺ in different deposition time. Inset: the calibration curve of Cd²⁺ and Pb²⁺ in different deposition time.

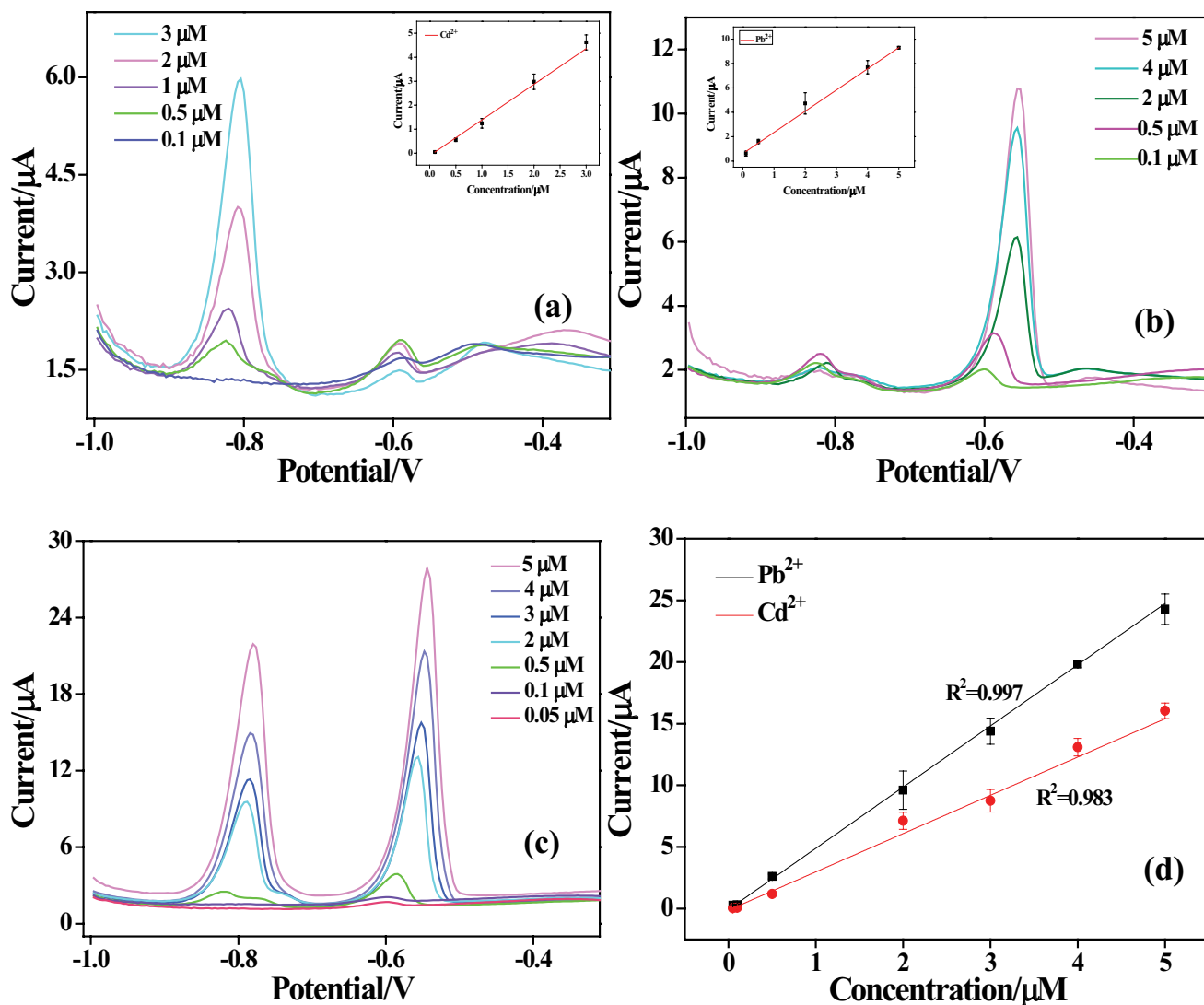


Fig. 10. (a) DPASV current responses of Cd^{2+} at 0.1, 0.5, 1.0, 2.0, and 3.0 μM with co-existent 0.3 μM Pb^{2+} . Inset: the calibration curve of Cd^{2+} , (b) DPASV current responses of Pb^{2+} at 0.1, 0.5, 2.0, 4.0, and 5.0 μM with co-existent 0.5 μM Cd^{2+} . Inset: the calibration curve of Pb^{2+} , (c) DPASV current responses, and (d) the calibration curve for simultaneous detection of Pb^{2+} and Cd^{2+} at 0.05, 0.1, 0.5, 2.0, 3.0, 4.0, and 5.0 μM , respectively.

Table 1
Comparison of electrochemical sensors reported with OM-MOF/GCE

	Linear range (μM)		LOD (μM)		Sensitivity ($\mu\text{A}/\mu\text{M}$)		Reference
	Pb^{2+}	Cd^{2+}	Pb^{2+}	Cd^{2+}	Pb^{2+}	Cd^{2+}	
CB-15-crown-5/GCE	0.05–0.90	0.14–1.70	0.02	0.04	2.91	1.23	[22]
In-situ Sb/SPCE	0.08–0.30	0.10–0.60	0.02	0.04	47.9	82.5	[23]
SbF/GO/SPCE	0.10–1.5	0.10–1.5	0.026	0.054	26.4	10.2	[24]
Nafion/CLS/PGR/GCE	0.05–5	0.05–5	0.01	0.003	0.775	2.12	[25]
NG/GCE	0.01–9	0.05–1,008	0.005	0.050	4.52	2.84	[26]
CS-Mn(TPA)-SWCNTs/GCE	0.01–14	–	0.038	–	3.35	–	[21]
Pd1.5/PAC-900/GCE	0.5–5.5	0.5–8.9	0.041	0.050	3.80	4.71	[27]
OM-MOF/GCE	0.05–5	0.05–5	0.013	0.038	4.96	3.07	This work

3 μM Pb^{2+} and 3 μM Cd^{2+} (Fig. 11a). The current responses were changed less than $\pm 10\%$ after adding 3 μM Mn^{2+} , Zn^{2+} ; 30 μM Ni^{2+} , Ca^{2+} , Mg^{2+} , and 60 μM Na^+ , K^+ , Cl^- , NO_3^- , which showed good anti-interference capability.

In order to make a thorough inquiry of stability and reproducibility of different parallel electrodes, five electrodes modified with the same modified solution (2 mg mL^{-1} OM-MOF, 8 μL) were detected by DPASV. As displayed in

Fig. 11b, the RSD of Pb^{2+} and Cd^{2+} was 4.5% and 7.1%, respectively, which reveals that different parallel electrodes owned good reproducibility in Pb^{2+} and Cd^{2+} detection.

The stability of modified material and modified electrodes was investigated by five times parallel determination in 1 d and in five consecutive days. As shown in Fig. 11c, the current signals in 1 d changed little with the standard deviation of 5.1% and 3.7% for Pb^{2+} and Cd^{2+} , respectively.

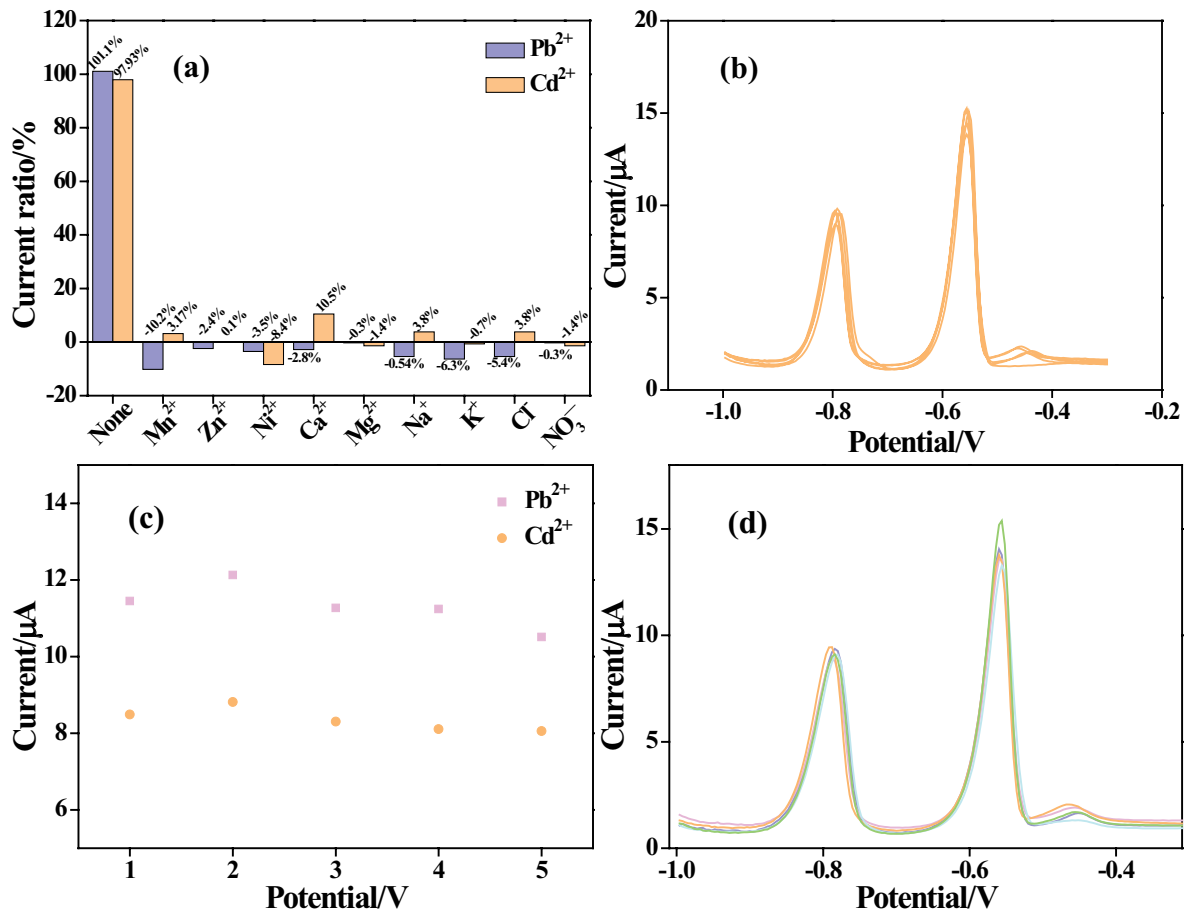


Fig. 11. (a) Interference of different kinds of ions in Pb^{2+} and Cd^{2+} detection, (b) current signal for different parallel electrodes ($n = 5$), (c) intraday parallel, and (d) daytime parallel determination, $n = 5$.

Table 2
Simultaneous detection of Pb^{2+} and Cd^{2+} in actual water samples

	Pb^{2+}			Cd^{2+}		
	Added (μM)	Found (μM)	Recovery (%)	Added (μM)	Found (μM)	Recovery (%)
Tap water	0	–	–	0	–	–
	2	1.96	98.2	2	2.01	100.7
	3	2.65	88.2	3	2.72	90.6
	4	4.05	101.2	4	3.50	87.0
River water	0	–	–	0	–	–
	2	1.86	93.0	2	2.20	110
	3	2.53	84.0	3	3.30	110
	4	3.82	95.4	4	3.44	85.6

To explore the consistency of modified electrodes, experiments were carried out within 5 d on one same electrode with acceptable RSD = 6.7% and 3.6% for Pb²⁺ and Cd²⁺, respectively (Fig. 11d). The above results suggested that the modified material and electrodes had reliable stability that could be utilized in ions detection.

3.6. Real sample detection

The application of OM-MOF/GCE was investigated by conducting Pb²⁺ and Cd²⁺ in top water and river water. As exhibited in Table 2, the recovery range of Pb²⁺ was 88.2%–101.2% in top water and 84.0%–95.4% in river water. Meanwhile, the recovery range of Cd²⁺ was 87.0%–100.7% in top water and 85.6%–110% in river water. The results showed above indicated that this sensor had better accuracy for test Pb²⁺ and Cd²⁺ in top water rather than in river water, which may attribute to less interferences in top water. However, the recoveries for both actual samples were within tolerance, confirming that the OM-MOF/GCE had relatively good accuracy for simultaneous detection of Pb²⁺ and Cd²⁺ in these two actual samples.

4. Conclusion

Summarily speaking, manganese-based metal-organic frameworks-oxidized MWCNTs composite (OM-MOF) was prepared by solvothermal synthesis methods. The composite was used as an electrode material for simultaneous detection of Pb²⁺ and Cd²⁺. The experiment conditions including material concentration, buffer solution types, buffer pH, deposition potential and deposition time were optimized and all experiments were conducted under material concentration: 2 mg mL⁻¹; supporting electrolyte: NaAc-HAc; optimal pH: 4.0; deposition time: 300 s; deposition potential: -1.2 V. Linear was investigated from 0.05 to 5 μM with low detection limit of 13 and 38 nM for Pb²⁺ and Cd²⁺, respectively. Meanwhile, this sensor showed admirable anti-interference, stability and reproducibility. The real sample detection showed a reasonable result, which suggested that this electrochemical sensor had well reliability and good practical applications.

Acknowledgments

This work was supported by the National Natural Science Foundation of China (No. 21571191 and (No. 51674292) and Key Laboratory of Hunan Province for Water Environment and Agriculture Product Safety (2018TP1003).

References

- [1] F. Zhou, X. Feng, J. Yu, X. Jiang, High performance of 3D porous graphene/lignin/sodium alginate composite for adsorption of Cd²⁺ and Pb²⁺, *Environ. Sci. Pollut. Res.*, 25 (2018) 15651–15661.
- [2] C. Liang, X. Feng, J. Yu, X. Jiang, Facile one-step hydrothermal syntheses of graphene oxide-MnO₂ composite and their application in removing heavy metal ions, *Micro Nano Lett.*, 13 (2018) 1179–1184.
- [3] B.-Y. Yue, L.-Y. Yu, F.-P. Jiao, X.-Y. Jiang, J.-G. Yu, The fabrication of pentaerythritol pillared graphene oxide composite and its adsorption performance towards metal ions from aqueous solutions, *Desal. Wat. Treat.*, 102 (2018) 124–133.
- [4] X. Shi, W. Gu, C. Zhang, L. Zhao, L. Li, W. Peng, Y. Xian, Construction of a graphene/Au-nanoparticles/cucurbit[7]uril-based sensor for Pb²⁺ sensing, *Chem. Eur. J.*, 22 (2016) 5643–5648.
- [5] J. Yang, J.H. Yu, J. Rudi Strickler, W.J. Chang, S. Gunasekaran, Nickel nanoparticle-chitosan-reduced graphene oxide-modified screen-printed electrodes for enzyme-free glucose sensing in portable microfluidic devices, *Biosens. Bioelectron.*, 47 (2013) 530–538.
- [6] D. Wang, Y. Ke, D. Guo, H. Guo, J. Chen, W. Weng, Facile fabrication of cauliflower-like MIL-100(Cr) and its simultaneous determination of Cd²⁺, Pb²⁺, Cu²⁺ and Hg²⁺ from aqueous solution, *Sens. Actuators, B*, 216 (2015) 504–510.
- [7] T. Priya, N. Dhanalakshmi, S. Thennarasu, N. Thinakaran, A novel voltammetric sensor for the simultaneous detection of Cd²⁺ and Pb²⁺ using graphene oxide/κ-carrageenan/l-cysteine nanocomposite, *Carbohydr. Polym.*, 182 (2018) 199–206.
- [8] S.-F. Zhou, X.-J. Han, H.-L. Fan, Q.-X. Zhang, Y.-Q. Liu, Electrochemical detection of As(III) through mesoporous MnFe₂O₄ nanocrystal clusters by square wave stripping voltammetry, *Electrochim. Acta*, 174 (2015) 1160–1166.
- [9] X.-J. Han, S.-F. Zhou, H.-L. Fan, Q.-X. Zhang, Y.-Q. Liu, Mesoporous MnFe₂O₄ nanocrystal clusters for electrochemistry detection of lead by stripping voltammetry, *J. Electroanal. Chem.*, 755 (2015) 203–209.
- [10] S.-F. Zhou, X.-J. Han, H.-L. Fan, J. Huang, Y.-Q. Liu, Enhanced electrochemical performance for sensing Pb(II) based on graphene oxide incorporated mesoporous MnFe₂O₄ nanocomposites, *J. Alloys Compd.*, 747 (2018) 447–454.
- [11] S.-F. Zhou, J.-J. Wang, L. Gan, X.-J. Han, H.-L. Fan, L.-Y. Mei, J. Huang, Y.-Q. Liu, Individual and simultaneous electrochemical detection toward heavy metal ions based on L-cysteine modified mesoporous MnFe₂O₄ nanocrystal clusters, *J. Alloys Compd.*, 721 (2017) 492–500.
- [12] S.-F. Zhou, X.-J. Han, Y.-Q. Liu, SWASV performance toward heavy metal ions based on a high-activity and simple magnetic chitosan sensing nanomaterials, *J. Alloys Compd.*, 684 (2016) 1–7.
- [13] H. Guo, Z. Zheng, Y. Zhang, H. Lin, Q. Xu, Highly selective detection of Pb²⁺ by a nanoscale Ni-based metal-organic framework fabricated through one-pot hydrothermal reaction, *Sens. Actuators, B*, 248 (2017) 430–436.
- [14] Y. Wang, L. Wang, W. Huang, T. Zhang, X. Hu, J.A. Perman, S. Ma, A metal-organic framework and conducting polymer based electrochemical sensor for high performance cadmium ion detection, *J. Mater. Chem. A*, 5 (2017) 8385–8393.
- [15] J. Guo, Y. Chai, R. Yuan, Z. Song, Z. Zou, Lead (II) carbon paste electrode based on derivatized multi-walled carbon nanotubes: Application to lead content determination in environmental samples, *Sens. Actuators, B*, 155 (2011) 639–645.
- [16] T. Ladrak, S. Smulders, O. Roubeau, S.J. Teat, P. Gamez, J. Reedijk, Manganese-based metal-organic frameworks as heterogeneous catalysts for the cyanosilylation of acetaldehyde, *Eur. J. Inorg. Chem.*, 2010 (2010) 3804–3812.
- [17] Y. Wang, Y. Wu, J. Xie, H. Ge, X. Hu, Multi-walled carbon nanotubes and metal-organic framework nanocomposites as novel hybrid electrode materials for the determination of nano-molar levels of lead in a lab-on-valve format, *Analyst*, 138 (2013) 5113–5120.
- [18] V. Guzsvány, O. Vajdle, M. Gurdeljević, Z. Kónya, Ag or Au nanoparticles decorated multiwalled carbon nanotubes coated carbon paste electrodes for amperometric determination of H₂O₂, *Top. Catal.*, 61 (2018) 1350–1361.
- [19] M. Shahbakhsh, S. Narouie, M. Noroozifar, Modified glassy carbon electrode with polydopamine-multiwalled carbon nanotubes for simultaneous electrochemical determination of biocompounds in biological fluids, *J. Pharm. Biomed. Anal.*, 161 (2018) 66–72.
- [20] M.S. Ahmad, I.M. Isa, N. Hashim, S.M. Si, M.I. Saidin, A highly sensitive sensor of paracetamol based on zinc-layered hydroxide-L-phenylalanate-modified multiwalled carbon nanotube paste electrode, *J. Solid State Electrochem.*, 22 (2018) 2691–2701.

- [21] F. Cai, Q. Wang, X. Chen, W. Qiu, F. Zhan, F. Gao, Q. Wang, Selective binding of Pb^{2+} with manganese-terephthalic acid MOF/SWCNTs: theoretical modeling, experimental study and electroanalytical application, *Biosens. Bioelectron.*, 98 (2017) 310–316.
- [22] N. Serrano, A. González-Calabuig, M. Del Valle, Crown ether-modified electrodes for the simultaneous stripping voltammetric determination of Cd^{2+} , Pb^{2+} and Cu^{2+} , *Talanta*, 138 (2015) 130–137.
- [23] V. Sosa, C. Barcelo, N. Serrano, C. Arino, J.M. Diaz-Cruz, M. Esteban, Antimony film screen-printed carbon electrode for stripping analysis of Cd^{2+} , Pb^{2+} , and Cu^{2+} in natural samples, *Anal. Chim. Acta*, 855 (2015) 34–40.
- [24] P. Ruengpirasiri, E. Punrat, O. Chailapakul, S. Chuanuwatanakul, Graphene oxide-modified electrode coated with in-situ antimony film for the simultaneous determination of heavy metals by sequential injection-anodic stripping voltammetry, *Electroanalysis*, 29 (2017) 1022–1030.
- [25] L. Yu, Q. Zhang, B. Yang, Q. Xu, Q. Xu, X. Hu, Electrochemical sensor construction based on Nafion/calcium lignosulphonate functionalized porous graphene nanocomposite and its application for simultaneous detection of trace Pb^{2+} and Cd^{2+} , *Sens. Actuators, B*, 259 (2018) 540–551.
- [26] H. Xing, J. Xu, X. Zhu, X. Duan, L. Lu, W. Wang, Y. Zhang, T. Yang, Highly sensitive simultaneous determination of cadmium (II), lead (II), copper (II), and mercury (II) ions on N-doped graphene modified electrode, *J. Electroanal. Chem.*, 760 (2016) 52–58.
- [27] P. Veerakumar, V. Veeramani, S.M. Chen, R. Madhu, S.B. Liu, Palladium nanoparticle incorporated porous activated carbon: electrochemical detection of toxic metal ions, *ACS Appl. Mater. Interfaces*, 8 (2016) 1319–1326.